

Comprehensive insights into the thermal and mechanical effects of metallic glasses via creep

Z.R. Xu^a, J.C. Qiao^{a,*}, J. Wang^b, E. Pineda^c, D. Crespo^{c,*}

^a*School of Mechanics, Civil Engineering and Architecture, Northwestern Polytechnical University, Xi'an 710072, China*

^b*State Key Laboratory of Solidification Processing, Northwestern Polytechnical University, Xi'an 710072, China*

^c*Department of Physics, Institute of Energy Technologies, Barcelona Research Center in Multiscale Science and Technology, Universitat Politècnica de Catalunya, 08019 Barcelona, Spain*

E-mail addresses: qjczy@nwpu.edu.cn

daniel.crespo@upc.edu

Submitted to *Journal of Materials Science & Technology*

(Version: May 28, 2021)

Abstract: Evolution of deformation and relaxation behaviors of a prototypical Cu₄₆Zr₄₆Al₈ metallic glass was explored by extensive creep tests under both physical aging and cyclic loading. Deep insights into the microstructure-induced dynamic heterogeneity which accommodates creep deformation were successively revealed via experimental measurements and spectral analyses. An annihilation of local defects within metallic glass with increasing annealing time and cyclic numbers was observed through the reduction of amplitude in both activation energy spectra and relaxation-time spectra, which were also accompanied by an ascending value of β_{KWW} . It is further found that the corresponding deformation units within the metallic glass do not

disappear permanently, but are recoverable over the course of cyclic loading. The apparent suppressed relaxation process can be gradually alleviated with increasing resuming time between two consecutive cycles, behaving differently from physical aging, which indicates a notable discrepancy between thermal treatment and mechanical treatment.

Keywords: Metallic glasses; Creep; Physical aging; Cyclic loading; Relaxation-time spectrum

1. Introduction

Due to their distinctive short-range ordered and long-range disordered structure, metallic glasses (MGs) show exceptional physical, chemical and mechanical properties in comparison with their crystalline counterparts [1-4]. In recent years, extensive experimental, computational, and theoretical studies have shown that the structural heterogeneity of MGs [5-9], which originates from their inhomogeneous atomic structure, is closely related to their glass transition, mechanical relaxation and crystallization behaviors, among other properties, which makes the research on the features of structural heterogeneity a subject of great significance [10-12].

In order to clarify the dynamic mechanical behavior of amorphous materials, various models have been proposed based on the concepts of free volume [13], shear transformation zones (STZs) [14], cooperative shear model [15, 16], quasi-point defects [17], liquid-like regions [18] or flow units [19]. Nevertheless, these models are virtually grounded on a mean-field theory, which appropriately simplify the intricate problem by introducing some effective critical physical parameters such as a mean activation volume or activation energy, resulting in a loss of vital information. A rationalized description of the deformation process of amorphous solids requires a sufficient and accurate introduction of dynamic heterogeneity, which is usually denoted by a wide distribution of activation energies or relaxation times of the corresponding deformation units.

As typical viscoelastic materials, the deformation behavior of amorphous solids

such as metallic glasses can be described by means of several fundamental spring and dashpot units connected in series or in parallel. Both the Maxwell and Kelvin (Voigt) models have been shown to be capable of characterizing the stress relaxation and creep process of MGs [20-23]. Furthermore, it is feasible to acquire a significant physical parameter τ which is defined as either the relaxation time or the retardation time, providing a simple method for quantifying the dynamical behavior. By introducing n Maxwell or Kelvin units, using the least square method, nonlinear regression method or other optimization methods, a relaxation-time spectrum can be finally obtained [24]. Due to the consideration of both dynamic mechanical behavior and the microstructural heterogeneity of MGs, the above method has been widely used in the study of the anelastic and viscoelastic behaviors of MGs [23, 25-27].

The conventional experimental approaches to explore the evolution of dynamic heterogeneity of MGs usually comprise dynamical mechanical analysis (DMA), stress relaxation and creep [5, 28-30]. DMA, by applying small alternating loads to the tested samples, supplies valid measures to accurately describe the viscoelastic behavior of MGs under dynamic loading. The time-, temperature- or driving frequency-dependent storage modulus E' and loss modulus E'' are also indicators directly reflecting the kinetic responses [5, 28, 31]. Besides, it enables us to clearly distinguish different forms of relaxation modes in MGs, i.e., primary (α) relaxation, secondary (β) relaxation and other types of relaxation modes [32, 33]. On the other hand, by means of stress relaxation, stress-time responses over a wide temperature range can be finally obtained. A power exponent fitted by the phenomenological KWW (Kohlrausch-William-Watts) equation is capable to present a visual and quantitative description for the dynamic heterogeneity within MGs [30, 34]. More recently, the two-stage process during stress relaxation of MGs has been widely reported, which corresponds to the transformation of deformation modes [30, 35]. The aforementioned multistage relaxation behavior of MGs has been denoted as a criterion of their dynamic heterogeneity.

Conversely, creep, loading the materials with constant stress while tracing the strain response, has proven to be a powerful tool for characterizing the dynamic heterogeneity as well as the distribution of microstructural heterogeneity in MGs. A large number of creep experiments have been conducted in MGs to investigate their

structural characteristics, energetic status and deformation mechanism supported by mathematical statistics and molecular dynamics simulation [12, 36, 37]. Retardation-time spectra were also extracted from nanoindentation creep tests to clarify the dynamic nature of MGs [25]. In addition, the creep process of MGs is closely related to such factors like external load, experimental temperature, loading time and so on, directly reflecting the true responses of MGs' microstructure under external stimuli. More intensive research of creep behavior of MGs is of great significance not only to contribute to understand their glass transition, deformation and structural relaxation behaviors but also to improve their service performance as engineering materials.

In the current work, a prototypical $\text{Cu}_{46}\text{Zr}_{46}\text{Al}_8$ (at.%) MG was chosen as a model alloy to explore the evolution of deformation and relaxation behaviors of amorphous solids by means of a series of creep tests. Two kinds of experimental conditions were adopted, one is changing the annealing time before the creep starts, the other is cyclic loading with different recovery durations. A generalized Kelvin model containing one Maxwell unit and n Kelvin units connected in series was used to analyze the creep behavior. The creep displacement, energy barrier distribution, stretching parameter β_{KWW} , characteristic relaxation time τ_i and its intensity ε_i under different conditions were discussed comparatively. Relaxation-time spectra were also obtained, endowing us with abundant detailed information about the dynamic heterogeneity within the specimens. Furthermore, the influence of physical aging and cyclic loading on creep behavior of $\text{Cu}_{46}\text{Zr}_{46}\text{Al}_8$ MG have also been systematically studied, which is helpful to clarify the underlying activation and evolution of deformation units under both thermal and mechanical stimuli, providing theoretical guidance for a thorough understanding of dynamic heterogeneity within MGs during creep.

2. Materials and experimental procedures

2.1 Sample preparation and structural characterization

The prototypical $\text{Cu}_{46}\text{Zr}_{46}\text{Al}_8$ bulk MG was fabricated by copper mold suction casting under a Ti-gettered argon atmosphere. The master alloy was re-melted at least 6 times to ensure its chemical homogeneity. In the current work, MG ribbons with width

about 1 mm and thickness about 30 μm were prepared by high-vacuum melt spinning from the master alloy.

The glassy nature of the alloy was verified by X-ray diffraction (XRD, D8 Bruker AXS GmbH) with Cu-K α radiation. The thermal properties of alloy were determined by differential scanning calorimeter (DSC, Netzsch 202) in a high-purity nitrogen atmosphere at a heating rate of 10 K/min.

2.2 Tensile creep experiment

The creep experiments of Cu₄₆Zr₄₆Al₈ MG ribbons were carried out using a commercial dynamic mechanical analyzer (DMA, TA Q800) in tensile mode at a temperature of 510 K ($T_g \sim 697$ K). To explore the effect of physical aging on creep, the specimens had been annealed at the same temperature during several aging times (from 0 min to 240 min). In the period of annealing, the tensile state of the ribbons was maintained by applying a small load of 0.001 N. After the annealing procedure, a constant tensile stress of 200 MPa was applied to the sample, and each creep test lasted for 10^5 s.

For cyclic creep tests, in every set of tests, 4 loading cycles were established and each lasted for 334 min (~ 20000 s). Between two cycles there was a recovery period which was changed systematically (from 0 min to 240 min). The corresponding creep tests were conducted at 510 K and 200 MPa after an initial equilibration of 5 min.

3. Results and discussion

3.1 The effect of the physical aging on creep

Fig. 1(a) exhibits the creep behavior of Cu₄₆Zr₄₆Al₈ MG ribbons under 200 MPa at a fixed temperature of 510 K with various aging times (from 0 min to 240 min). For a more intuitive view, the instantaneous elastic part was artificially removed. It can be seen that the strain increases first rapidly and then evolves more and more slowly with increasing time in all cases. Moreover, it shows a tendency that the longer the aging time, the weaker the amplitude of the transient creep, indicating a significant increase in stiffness of samples due to physical aging. As is well documented, the amorphous

solids tend to reach an iso-configurational steady state creep once the observing time is long enough [38]. Taking the slopes of the last 20000 s of the corresponding creep curves in Fig. 1, variation of steady-state strain rate of Cu₄₆Zr₄₆Al₈ MG with different aging times is calculated and shown in Fig. 2(a). It can be observed that the steady-state strain rate generally shows an insensitive characteristic with increasing aging time. This may be understood considering that subadjacent aging is also active during the creep tests, leading to a similar iso-configurational state, i.e. the same steady state rate, after long times.

The inhomogeneous deformation of MGs usually involves a coordinated rearrangement of corresponding single atoms or clusters, which need to be activated by crossing energy barriers. Behaving differently from conventional crystals, the energy barriers of MGs are widely spread over different scales [39]. Since the creep process excites the MG to a state of higher energy, distribution of energy barrier can be indirectly inferred via the observation of certain changes caused by the thermal activation process. According to the activation energy spectrum model, the variation of instantaneous strain ε on time t during creep can be expressed as [40]:

$$\Delta\varepsilon(t) = \int_0^{+\infty} p(E)\theta(E, T, t)dE \quad (1)$$

where $p(E)$ represents the number of energy barriers within the range of E to $E + dE$, $\theta(E, T, t)$ is a characteristic annealing function, of exponential form. Due to the existence of critical characteristic relaxation time τ_c and activation energy E_c during creep, only those deformation units with $\tau_c < t$ and $E < E_c$ participate in the creep process. Consequently, on the basis of step-like approximation, finally we got [41]:

$$P(E) = -\frac{1}{kT} \frac{d\varepsilon(t)}{d\ln t} \quad (2)$$

$$E = kT\ln(\nu_0 t) \quad (3)$$

taking k as the Boltzmann constant of 1.38×10^{-23} J K⁻¹, and ν_0 the Debye frequency of 10^{13} s⁻¹ [42]. The resulting apparent activation energy spectra are shown in Fig. 1(b), where $P(E)$ under each aging time is normalized by its corresponding peak value to further highlight the aging time dependence of spectral position and peak width. It can

be seen that the activation energies of deformation units are widely distributed, directly characterizing the dynamic heterogeneity of deformation units over the course of activation. Furthermore, the spectra shift toward a higher energy state with increasing aging time, which clearly indicates that the deformation units get harder to be activated at longer aging times. These results also provide a plausible explanation for the occurrence of suppressed relaxation behavior caused by physical aging which was previously mentioned.

To deeply understand the deformation dynamics, the creep curves are further fitted by a stretched exponential KWW equation [29, 39]:

$$\varepsilon(t) = \varepsilon_0 \left(1 - \exp \left(- \left(\frac{t}{\tau_c} \right)^{\beta_{KWW}} \right) \right) + \frac{t}{\mu_0} \quad (4)$$

with ε_0 being the pre-factor of strain, τ_c being the characteristic relaxation time indicating the release rate of the “delayed plasticity”, β_{KWW} being the stretching parameter ranging from 0 to 1, and μ_0 a constant obtained from the steady-state strain rate which is related to the longitudinal viscosity of each sample. Here, β_{KWW} describes the distribution width of relaxation times, which is a significant parameter that characterizes the dynamic heterogeneity of MGs. Fig. 2(b) shows the evolution of the parameters τ_c and β_{KWW} fitted by the KWW equation with various aging times. The characteristic relaxation time τ_c generally represents an upward tendency with increasing aging time, rising from a lower value of below 4000 s for the as-cast state to above 12000 s for the case of annealing for 240 min, which denotes that the deformation units are much more difficult to be activated after longer aging times. On the other hand, the stretching exponent β_{KWW} gradually increases from 0.43 to a higher value of about 0.70. It is widely accepted that β_{KWW} is a signature indirectly reflecting the structural heterogeneity of a MG system. As the value of β_{KWW} is closer to 1, the structure of MG tends to be more homogeneous, and it decreases as the heterogeneity increases. The process of physical aging below T_g induces the structural rearrangement of atoms, as a consequence, both the density and elastic modulus of MG increase. From a macroscopic point of view, the viscous flow and plastic deformation are harder to

activate. Combined with the evolution of activation energy spectra, it is reasonable to deduce that increasing aging time changes the MG system toward a more stable state, accompanied by a decrease of atomic mobility. Moreover, the atomic mobility in MGs corresponds to the concentration of “defects” (deformation units) inherent in their microstructure [43, 44]. However, unlike the structural defects such as grain boundaries, twins and dislocations in conventional crystals, the “defects” mentioned here refer to a class of micro-domains within MGs which possess looser atomic arrangement, lower modulus and higher atomic mobility. Although the exact definitions are slightly different based on various theoretical models, such as quasi-point defects [17], liquid-like regions [18], flow units [19], interstitial defects [45], etc., these concepts undoubtedly benefit for further understanding of the deformation mechanism of MGs. Here, we closely link the physical aging effect with the variation of the heterogeneous microstructure within of Cu₄₆Zr₄₆Al₈ MG, basing on the introduction considering that such heterogeneity is related to the presence of “defects”. Taking these results into consideration, one is capable to infer that a portion of “defects” (deformation units) previously available to participate in the creep process are annihilated during physical aging process. The longer the physical aging lasts, the larger volume fraction of deformation units are annihilated, ultimately resulting in a more homogeneous microstructure of MG specimens and, consequently, the apparent suppressed relaxation phenomenon as exhibited in Fig. 1(a).

The phenomenological KWW model can quantitatively describe the time-dependent evolution of dynamic heterogeneity of MGs during creep. Unfortunately, it fails to accurately reflect the distribution of events at different temporal scales. Based on the recent research and experimental observation of microstructure heterogeneity, MGs can be considered to consist of an elastic matrix and a set of scattered deformation units (as is schematically displayed in Fig. 3(a)), whose characteristic relaxation time τ_i can span several orders of magnitude [20, 42, 46]. Under the condition that the applied stress is much lower than the yield stress, the interaction between deformation units could almost be ignored [42]. Thereby, a generalized Kelvin model is able to describe the creep process of MGs, the spring units obeying Hooke’s law represent the

elastic matrix and the dashpot units following Newton's law are an adequate description of the deformation units. In the present work, a constitutive model containing a Maxwell unit and n Kelvin units connected mutually in series is utilized. As illustrated in Fig. 3(b), the linear spring unit E_{el} represents the instantaneous elastic component of MGs, while the dashpot unit η_v represents the viscoplastic component and the Kelvin units consisting of a spring unit E_i and a dashpot unit η_i in parallel, thus determining a characteristic relaxation time τ_i , stand for the viscoelastic (or anelastic) behavior. By means of this model, without considering the instantaneous elastic deformation, the displacement during the creep process can be expressed as:

$$\varepsilon(t) = \sum_{i=1}^n \frac{\sigma_0}{E_i} \left(1 - \exp\left(-\frac{t}{\tau_i}\right) \right) + \frac{t}{\mu_0} \quad (5)$$

where $\tau_i = \frac{\eta_i}{E_i}$ characterizes the relaxation time for the activation of the i th deformation unit and σ_0 is the applied stress.

For the sake of both ~~brevity~~brevity-simplicity and accuracy, we finally take $n=4$, the creep curves of Cu₄₆Zr₄₆Al₈ MG can be precisely fitted with Eq. (5). The variation of characteristic relaxation times τ_i with various aging times is exhibited in Fig. 2(c), and the radius of symbols representing τ_i are proportional to the intensity of the corresponding pre-exponential factors ε_i calculated by $\frac{\sigma_0}{E_i}$. It can be seen that τ_i tends to take values of about 40 s, 350 s, 3000 s and 17000 s, respectively, the value of which spans several orders of magnitude, implying a broad distribution in temporal scale of diverse deformation units and directly reflecting the dynamic heterogeneity of MGs during the creep process. Moreover, the generalized Kelvin model adequately characterizes the creep behavior, which demonstrates that the intrinsic dynamic heterogeneity of MGs is likely to arise from their microstructural inhomogeneity. On the other hand, as is shown in Fig. 2(c), the intensities of ε_1 and ε_3 are insensitive to creep time, whereas the intensity of ε_2 decreases while ε_4 increases dramatically with increasing aging time. Long relaxation time, i.e. τ_4 , is supposed to be associate with the possible anelastic response of MGs. The prolongation of relaxation time indicates that more deformation units shift to behave anelastically as aging time

increases. The reduction of the transient creep strength can be then associated to the decrease of deformation units with short time scale τ_2 during aging. Small and fast-activated deformation units within MG specimens are initially annihilated during physical aging process, while the remaining deformation units tend to take larger dimensions and longer characteristic relaxation times, making them much more difficult to be activated. This is also the origin of the increase of average time scale τ_c and dynamic heterogeneity β_{KWW} as displayed in Fig. 2.

3.2 The effect of cyclic loading on creep

In addition to physical aging, mechanical fatigue is another common situation inevitably faced by MGs during their service [47, 48]. Thus, a series of cyclic creep experiments were successively carried out to investigate the evolution of both structural and mechanical properties of MGs under cyclic loading. 4 repeated loading cycles were conducted on Cu₄₆Zr₄₆Al₈ MG ribbons, and in all cases the reloading process lasted for 334 min (~20000 s) at a constant temperature of 510 K and a fixed applied stress of 200 MPa. Fig. 4 endows a description of the entire experimental process and precisely shows the variation of measured strain and length of the ribbon as a function of time with a resuming time of 60 min. It can be seen that at the moment of loading (unloading), the curve appears to increase (decline) abruptly, reflecting the instantaneous elastic response of the specimen. Besides, both the overall length and strain of the specimen becomes progressively smaller during the recovery process, characterizing the unique anelastic properties of glassy state materials.

The strain-time curves of Cu₄₆Zr₄₆Al₈ MG ribbons under the influence of both resuming time and number of loading cycles are exhibited in Fig. 5. Several experimental results can be summarized as follows: During the creep process, as displayed in Fig. 5(a), the creep curves of the specimen gradually shift toward a lower strain rate with the increase of cyclic loading numbers, and the difference between two consecutive curves gets smaller and smaller, denoting that the cyclic loading treatment results in less effect on creep with increasing number of cycles. Similar phenomena can be observed during the recovery stage, as shown in Fig. 5(b). On the other hand, as seen

in Fig. 5(c), larger anelastic displacements are observed with the gradual prolongation of the interval time between two loadings. Compared with that without the treatment of cyclic loading (as shown in Fig. 1(a)), an iso-configurational steady state is earlier entered, which indicates a significant effect of cyclic loading on the creep behavior of $\text{Cu}_{46}\text{Zr}_{46}\text{Al}_8$ ribbons. As for the recovery stage after unloading, the anelastic deformation is insensitive to the resuming time, merely a small-scale hysteresis occurs when the interval time is long enough (>30 min).

In order to obtain further information on the evolution of activation energy of specimens under cyclic loading, using the method previously mentioned in the last section, activation energy spectra during cyclic loading process are calculated and displayed in Fig. 6. All curves are normalized using the corresponding peak value of the first loading stage. Fig. 6(a) exhibits the normalized activation energy spectra for 4 successive cyclic loadings with a resuming time of 60 min. Due to the limited testing time of each creep experiment, the deformation units with an activation energy barrier higher than $kT\ln(\nu_0 t)$ will not be involved in the creep process, and thus merely partial energy spectrum can be obtained during the subsequent loading stage. The intensity of spectra decreases with the ascending cyclic numbers, clearly indicating that the number of deformation units participating in each energy interval gradually decreases, accompanied by an increasing activation energy barrier. On the other hand, Fig. 6(b) displays the evolution of normalized energy spectra under the influence of resuming time. **During the 4th loading stage**, as the resuming time between two adjacent cycles increases from 0 min to 240 min, the intensity of spectrum presents an increasing trend. This fact denotes a recovery process underwent by deformation units during the unloading stage, which is more obvious with increasing resuming time. Furthermore, by integrating the activation energy spectrum, a relative deformation units concentration that activated in each creep cycle can be obtained. It can be seen from Fig. 6(c) that in all cases the concentration decreases exponentially with the number of cycles. With the gradual prolongation of the resuming time, a higher concentration of deformation unit is observed. However, once the resuming time is long enough (>60 min), as shown in the illustration, the impact of a longer recovery process becomes

insignificant. For the case with a resuming time of 240 min, the concentration ultimately approaches a low value of about 0.02, instead of tending toward 0, which denotes a mutual effect of resuming time as well as number of cycles on the specimen over the course of cyclic loading, the consumption and recovery of deformation units eventually reaches a certain dynamic equilibrium.

A phenomenological KWW model is sequentially adopted with the hope of obtaining more information which could quantitatively describe the evolution of dynamic heterogeneity of Cu₄₆Zr₄₆Al₈ ribbons during the process of cyclic loading. Fig. 6(d) displays the variation of the fitted KWW parameter β_{KWW} during creep process with various resuming times (from 5 min to 240 min) as well as number of loading cycles (from 1 to 4). Since the initial conditions of every experiment remain the same, the β_{KWW} is always found around a low value of 0.39 during the first loading, which also reflects the accuracy and reproducibility of the experimental results. Taking account of both the macroscopic deformation response and the evolution of activation energy spectra of materials, it can be inferred that the deformation units inside the specimen are gradually exhausted over the course of cyclic loading, which is similar to the effect of physical aging. Hence, it leads to a more homogeneous microstructure within the system and, therefore, a higher β_{KWW} value. On the other hand, a decreasing tendency of β_{KWW} with increasing resuming time between two loading cycles can be directly observed, indicating the recovery process underwent by the corresponding deformation units.

In addition to the KWW fitting, a discrete spectrum analysis was adopted for investigating the response of Cu₄₆Zr₄₆Al₈ MG under loading cycles at a broader temporal scale. Since the creep behavior in successive loading cycles identically obeys the basic law of creep, the same generalized Kelvin model was utilized. Due to the fact that different terms of the corresponding constitutive equation differ significantly in magnitude, a stress-strain relationship of derivative type was finally applied which can be expressed as:

$$\frac{d\varepsilon}{dt} = \sum_{i=0}^n \frac{\varepsilon_i}{\tau_i} \left(\exp\left(-\frac{t}{\tau_i}\right) \right) + \frac{\sigma_0}{\eta_v} \quad (6)$$

where τ_i characterizes the relaxation time of the i th deformation unit and ε_i is the amplitude of corresponding relaxation time τ_i . Considering that each creep process lasts 20000 s, the characteristic relaxation time of corresponding deformation units within MG was estimated to span over 6 orders of magnitude. Minimization was conducted by means of the least square fitting method. The relaxation time distributions obtained are shown in Fig. 7, all plots are normalized to the highest peak value for the sake of clarity. Similar to the previous analysis, the relaxation spectrum of the first cycle is notably broad for the short resuming times, once the stress is re-exerted again the corresponding deformation units contained in the specimen are mostly still deformed, this leading to a narrow relaxation spectrum formed only by the shortest times and a corresponding high value of β_{KWW} . On the other hand, with the increasing time interval between two adjacent loadings, the deformed reversible units have time to relax and be activated again during the subsequent loading. This leads to a more widely distributed relaxation time spectrum, a larger concentration of deformation units, and then a decrease of β_{KWW} . Nevertheless, as already noted before, the results suggest that the change of the relaxation time distribution after consecutive cycles becomes smaller as the number of cycles increases, the significant change being between the first and the second cycle.

Taking all obtained results into consideration, we attempt to reveal the physical nature of the above phenomena appearing during physical aging and cyclic loading. As is schematically illustrated in Fig. 8(a), the scattered deformation units will transform into elastic matrix during physical aging, and the units with lower energy barriers and shorter relaxation times take the lead in this transition. As the physical aging process proceeds, more units with larger relaxation times participate in this transformation. The remaining units tend to possess much higher atomic stacking densities and rather finite capacities accommodating to creep deformation, which causes a transition from fast-relaxation to slow-relaxation underwent by MGs. With regard to the cyclic loading process, as seen in Fig. 8(b), the deformation units are shear transformed under applied stress and part of them will flip backward once the stress is removed [49, 50]. Since the rate of backward flipping of deformation units within the system is much slower in

comparison with the rate of forward transformation, the final result is the gradually exhaustion of the deformation units during the cyclic creep. This effect induces a restriction of the relaxation behavior and leads to the apparent hardening phenomenon as displayed in Fig. 5(a). The following re-loading process, resulting from the backward flipping of previously shear transformed deformation units, is strongly related to the time interval between each cycle. Fast-activated units, with smaller dimensions and shorter relaxation times, act as pioneer in shear transforming during loading process. Once the applied stress is removed, they revert to a relaxed state immediately, and then contribute to the next deformation process, resulting in a relative fast relaxation process. Consequently, narrow relaxation spectra formed only by rather shorter relaxation times are detected. As the resuming time increases, more deformation units with longer relaxation times become recoverable and then involve in the subsequent cycle of creep, which is specifically manifested as a more widely distributed relaxation time spectrum as well as an alleviation of the transient creep suppression phenomenon. Nevertheless, the reactivation of corresponding deformation units occurs locally and is somewhat limited, the process between backward flipping and positive shear transformation of deformation units tends to reach a quasi-equilibrium state at sufficient large loading cycles and long resuming times, thus resulting in a stable level of dynamic heterogeneity within MG.

4. Conclusion

In summary, the evolution of deformation and relaxation behaviors of a prototypical Zr-based MG was explored by extensive creep tests under physical aging and cyclic loading. Deep insights into the microstructure-induced dynamic heterogeneity that accommodates creep deformation of MGs were obtained by means of experimental measurements and theoretical models. Under the frame of the generalized Kelvin model, relaxation-time spectra were further utilized to quantitatively describe the time scales involve in the creep of MGs. An annihilation of local deformation units during physical aging and cyclic loading was detected through the diminution of amplitude in both activation energy and relaxation-time spectra,

accompanied by an increasing value of β_{KWW} . Eventually, a structurally more stable state is reached by MGs, whose ability to resist deformation is weakened due to the progressive reduction of these deformation units. Nevertheless, unlike the annealing treatment, deformation units do not vanish permanently during the cyclic loading process and can gradually be recovered after removing the applied stress, indicating a notable discrepancy between thermal treatment and mechanical treatment for MGs. The present work is helpful to clarify the underlying activation and evolution of deformation units over the course of physical aging and cyclic loading, providing an alternative method, in addition to traditional DMA and stress relaxation, to quantitatively probe the intrinsic dynamic heterogeneity of MGs.

Acknowledgments

This work is supported by the NSFC (Grant No. 51971178), the Natural Science Basic Research Plan for Distinguished Young Scholars in Shaanxi Province (Grant No. 2021JC-12) and the fund of the State Key Laboratory of Solidification Processing in NWPU (Grant No. SKLSP202017). E. Pineda and D. Crespo acknowledge financial support from MICINN (grant FIS2017-82625-P) and Generalitat de Catalunya (grant 2017SGR0042).

References

- [1] W.H. Wang, Prog. Mater. Sci. 57 (2012) 487-656.
- [2] Y. Wu, H. Bei, Y.L. Wang, Z.P. Lu, E.P. George, Y.F. Gao, Int. J. Plast. 71 (2015) 136-145.
- [3] T.C. Hufnagel, C.A. Schuh, M.L. Falk, Acta Mater. 109 (2016) 375-393.
- [4] C. Schuh, T. Hufnagel, U. Ramamurty, Acta Mater. 55 (2007) 4067-4109.
- [5] J.C. Qiao, Q. Wang, J.M. Pelletier, H. Kato, R. Casalini, D. Crespo, E. Pineda, Y. Yao, Y. Yang, Prog. Mater. Sci. 104 (2019) 250-329.
- [6] H. Wagner, D. Bedorf, S. Kuchemann, M. Schwabe, B. Zhang, W. Arnold, K. Samwer, Nat. Mater. 10 (2011) 439-442.
- [7] Y.H. Liu, D. Wang, K. Nakajima, W. Zhang, A. Hirata, T. Nishi, A. Inoue, M.W. Chen, Phys. Rev. Lett. 106 (2011) 125504.
- [8] A. Hirata, L.J. Kang, T. Fujita, B. Klumov, K. Matsue, M. Kotani, A.R. Yavari, M.W. Chen, Science 341 (2013) 376-379.
- [9] Q. An, K. Samwer, M.D. Demetriou, M.C. Floyd, D.O. Duggins, W.L. Johnson, W.A. Goddard, Proc. Natl. Acad. Sci. U. S. A. 113 (2016) 7053-7058.

440 [10] Y.H. Liu, G. Wang, R.J. Wang, D.Q. Zhao, M.X. Pan, W.H. Wang, *Science* 315 (2007) 1385-1388.

441 [11] H.B. Yu, W.H. Wang, K. Samwer, *Mater. Today* 16 (2013) 183-191.

442 [12] P. Cao, M.P. Short, S. Yip, *Proc. Natl. Acad. Sci. U. S. A.* 114 (2017) 13631-13636.

443 [13] F. Spaepen, *Acta Metall.* 25 (1977) 407-415.

444 [14] A.S. Argon, *Acta Metall.* 27 (1979) 47-58.

445 [15] W.L. Johnson, K. Samwer, *Phys. Rev. Lett.* 95 (2005) 195501.

446 [16] J.S. Harmon, M.D. Demetriou, W.L. Johnson, K. Samwer, *Phys. Rev. Lett.* 99 (2007) 135502.

447 [17] J. Perez, *Solid State Ionics* 39 (1990) 69-79.

448 [18] T. Egami, *Prog. Mater. Sci.* 56 (2011) 637-653.

449 [19] Z. Lu, W. Jiao, W.H. Wang, H.Y. Bai, *Phys. Rev. Lett.* 113 (2014) 045501.

450 [20] W. Jiao, P. Wen, H.L. Peng, H.Y. Bai, B.A. Sun, W.H. Wang, *Appl. Phys. Lett.* 102 (2013) 101903.

451 [21] H.B. Ke, P. Zhang, B.A. Sun, P.G. Zhang, T.W. Liu, P.H. Chen, M. Wu, H.G. Huang, *J. Alloys*

452 *Compd.* 788 (2019) 391-396.

453 [22] F. Spaepen, *J. Mater. Sci.* 16 (1981) 3087-3092.

454 [23] J.D. Ju, D. Jang, A. Nwankpa, M. Atzmon, *J. Appl. Phys.* 109 (2011) 053522.

455 [24] J.R. Cost, *J. Appl. Phys.* 54 (1983) 2137-2146.

456 [25] A. Castellero, B. Moser, D.I. Uhlenhaut, F.H. Dalla Torre, J.F. Löffler, *Acta Mater.* 56 (2008)

457 3777-3785.

458 [26] Z. Lv, C. Yuan, H. Ke, B. Shen, *J. Mater. Sci. Technol.* 69 (2021) 42-47.

459 [27] T.J. Lei, L.R. DaCosta, M. Liu, W.H. Wang, Y.H. Sun, A.L. Greer, M. Atzmon, *Acta Mater.* 164

460 (2019) 165-170.

461 [28] J.C. Qiao, Y.J. Wang, J.M. Pelletier, L.M. Keer, M.E. Fine, Y. Yao, *Acta Mater.* 98 (2015) 43-50.

462 [29] Z. Wang, B.A. Sun, H.Y. Bai, W.H. Wang, *Nat. Commun.* 5 (2014) 5823.

463 [30] J.C. Qiao, Y.J. Wang, L.Z. Zhao, L.H. Dai, D. Crespo, J.M. Pelletier, L.M. Keer, Y. Yao, *Phys.*

464 *Rev. B* 94 (2016) 104203.

465 [31] H.B. Yu, K. Samwer, Y. Wu, W.H. Wang, *Phys. Rev. Lett.* 109 (2012) 095508.

466 [32] Q. Wang, S.T. Zhang, Y. Yang, Y.D. Dong, C.T. Liu, J. Lu, *Nat. Commun.* 6 (2015) 7876.

467 [33] H.B. Yu, W.H. Wang, H.Y. Bai, Y. Wu, M.W. Chen, *Phys. Rev. B* 81 (2010) 220201.

468 [34] P. Luo, M.X. Li, H.Y. Jiang, P. Wen, H.Y. Bai, W.H. Wang, *J. Appl. Phys.* 121 (2017) 135104.

469 [35] P. Luo, P. Wen, H.Y. Bai, B. Ruta, W.H. Wang, *Phys. Rev. Lett.* 118 (2017) 225901.

470 [36] C. Herrero-Gomez, K. Samwer, *Sci. Rep.* 6 (2016) 33503.

471 [37] J.O. Krispeneit, S. Pitikaris, K.E. Avila, S. Kuchemann, A. Kruger, K. Samwer, *Nat. Commun.* 5

472 (2014) 3616.

473 [38] M. Galano, G.H. Rubiolo, *Scr. Mater.* 48 (2003) 617-622.

474 [39] P.G. Debenedetti, F.H. Stillinger, *Nature* 410 (2001) 259-267.

475 [40] M.R.J. Gibbs, J.E. Evetts, J.A. Leake, *J. Mater. Sci.* 18 (1983) 278-288.

476 [41] S.V. Khonik, A.V. Granato, D.M. Joncich, A. Pompe, V.A. Khonik, *Phys. Rev. Lett.* 100 (2008)

477 065501.

478 [42] A.S. Argon, H.Y. Kuo, *J. Non-Cryst. Solids* 37 (1980) 241-266.

479 [43] J.C. Qiao, Y.H. Chen, R. Casalini, J.M. Pelletier, Y. Yao, *J. Mater. Sci. Technol.* 35 (2019) 982-

480 986.

481 [44] L.C.E. Struik, *Polym. Eng. Sci.* 17 (1977) 165-173.

482 [45] A.V. Granato, *Eur. Phys. J. B* 87 (2014) 1-6.

483 [46] J.C. Ye, J. Lu, C.T. Liu, Q. Wang, Y. Yang, *Nat. Mater.* 9 (2010) 619-623.

- 484 [47] B.C. Menzel, R.H. Dauskardt, *Acta Mater.* 54 (2006) 935-943.
485 [48] K.M. Flores, W.L. Johnson, R.H. Dauskardt, *Scr. Mater.* 49 (2003) 1181-1187.
486 [49] A. Lemaitre, C. Caroli, *Phys. Rev. Lett.* 103 (2009) 065501.
487 [50] W. Jiao, P. Wen, H.Y. Bai, Q.P. Kong, W.H. Wang, *Appl. Phys. Lett.* 103 (2013) 161902.
488

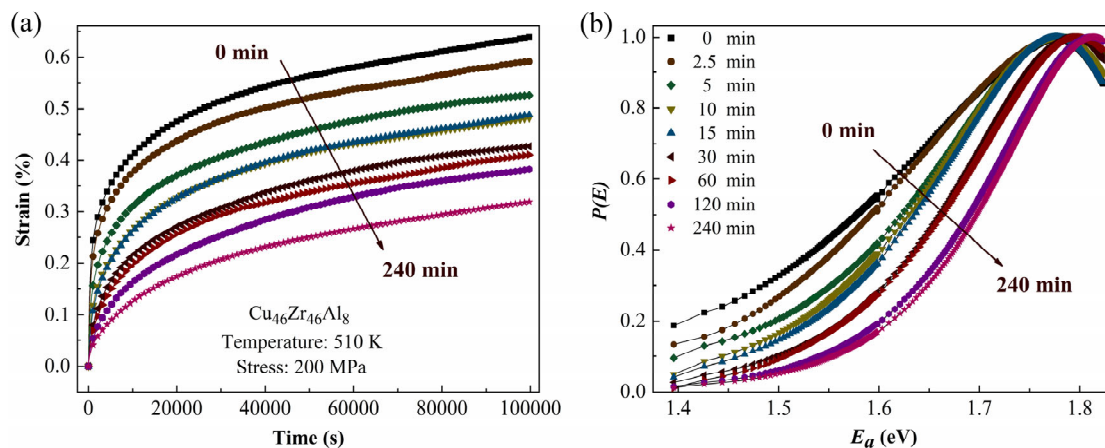
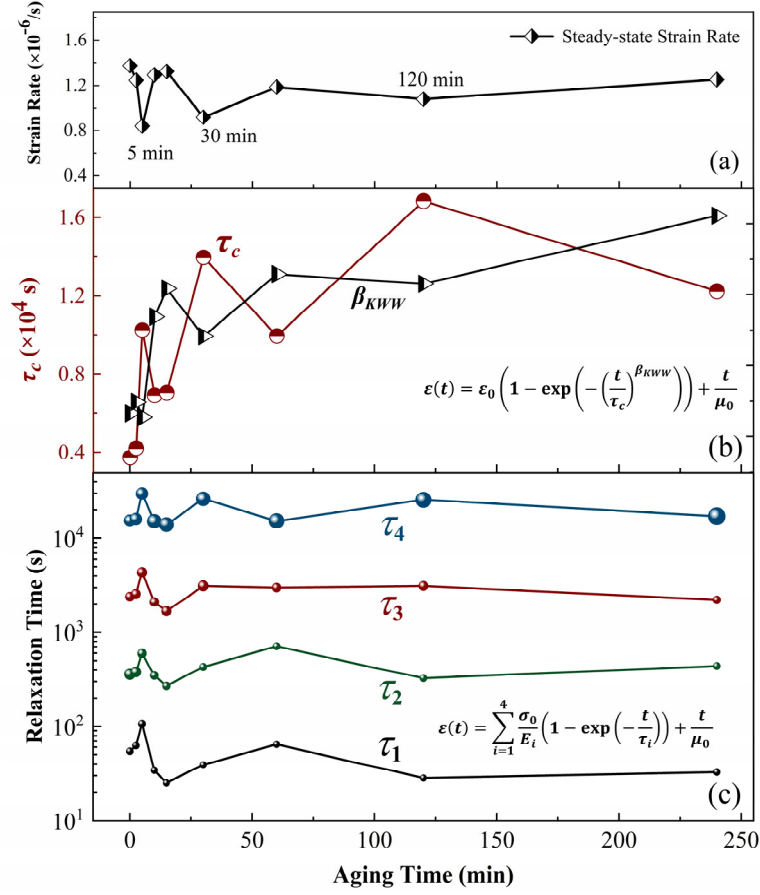


Fig. 1. (a) Creep strain as a function of time at a constant temperature $T=510$ K and a fixed applied stress $\sigma=200$ MPa. (The samples were annealed with different time (ranges from 0 min to 240 min) at 510 K); (b) Evolution of normalized activation energy spectra with aging time.



496

497 **Fig. 2.** (a) Variation of steady-state strain rate with different aging times; (b)
 498 Evolution of the characteristic relaxation time τ_c and the stretching parameter β_{KWW}
 499 fitted by KWW equation as a function of aging time; (c) Variation of characteristic
 500 relaxation time τ_i ($i=1, 2, 3$ and 4) fitted with Eq. (5), the radius of symbols
 501 representing τ_i are proportional to the corresponding intensity of pre-exponential
 502 factor ε_i calculated by $\frac{\sigma_0}{E_i}$.

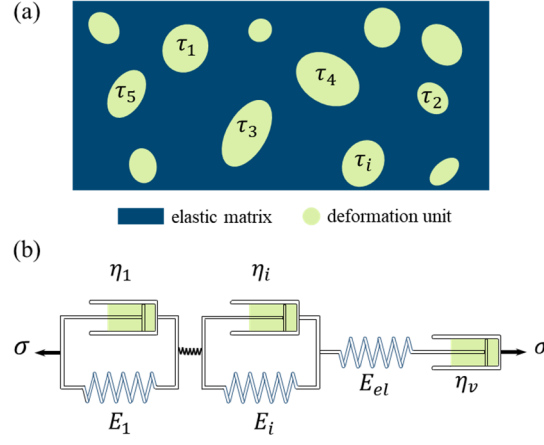


Fig. 3. (a) Schematic diagram of MGs composed of elastic matrix and scattered deformation units; (b) Schematic illustration of the generalized Kelvin model containing a Maxwell unit and n Kelvin units connected in series, where i -type sites correspond to modulus E_i , viscosity η_i and relaxation time $\tau_i = \frac{\eta_i}{E_i}$.

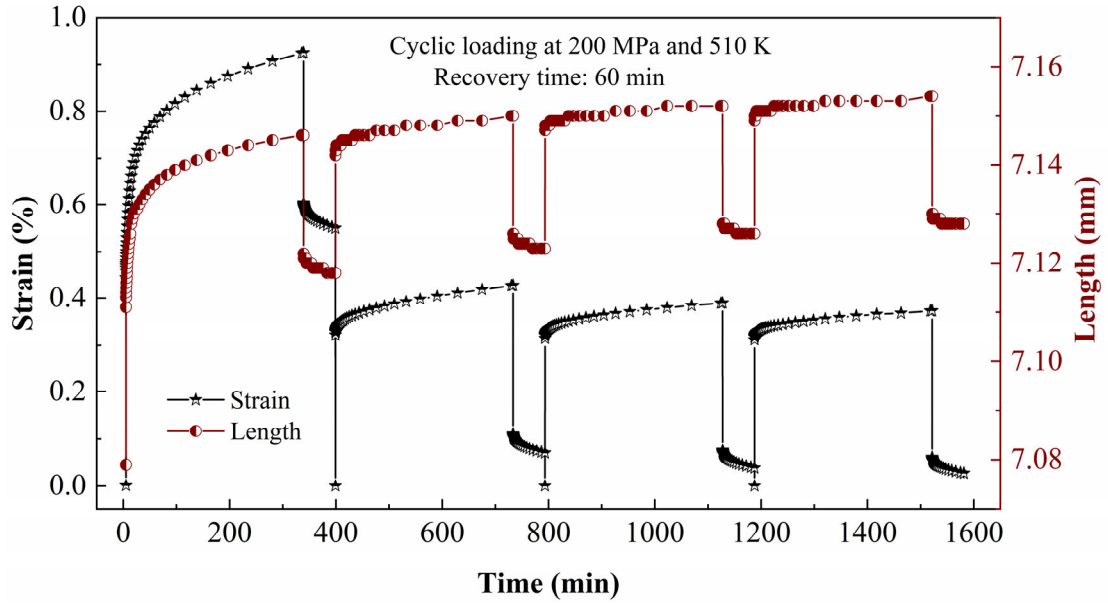


Fig. 4. Strain and measured length of the $\text{Cu}_{46}\text{Zr}_{46}\text{Al}_8$ ribbon as a function of time at a constant temperature of 510 K and a fixed applied stress of 200 MPa. (The sample was annealed at 510 K for 5 min and the recovery time between two loading cycles is 60 min)

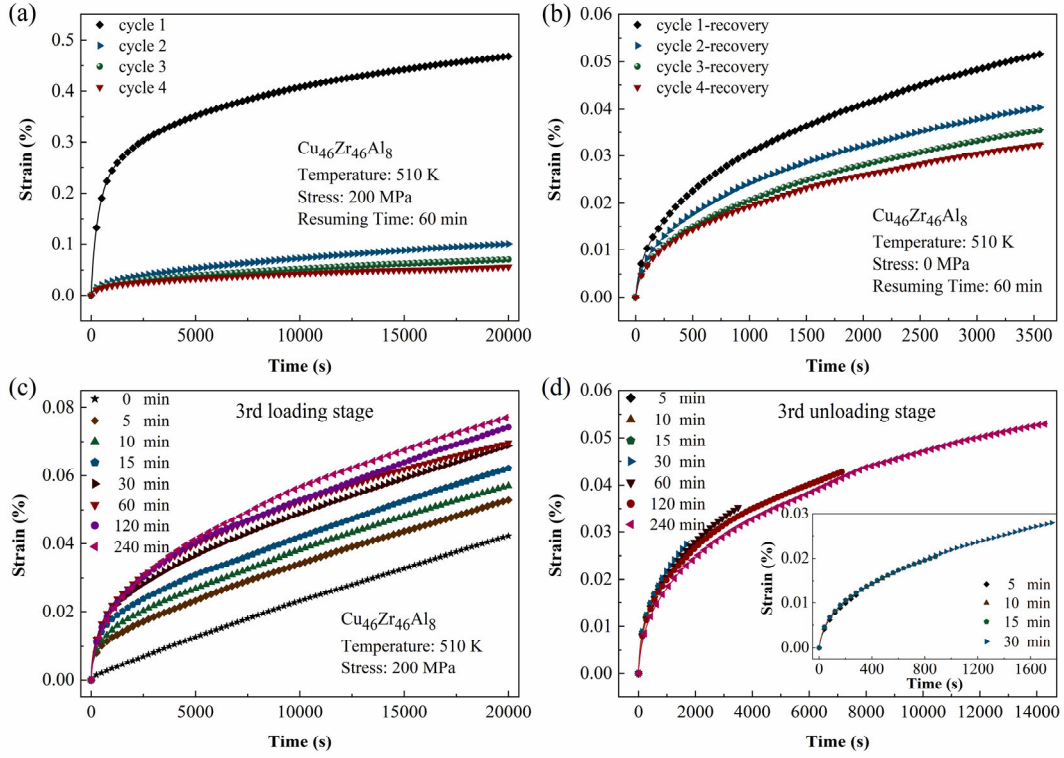


Fig. 5. (a) Cyclic creep curves of $\text{Cu}_{46}\text{Zr}_{46}\text{Al}_8$ MG with a resuming time of 60 min; (b) Recovery curves of $\text{Cu}_{46}\text{Zr}_{46}\text{Al}_8$ MG with a resuming time of 60 min; (c) Variation of creep strain after various resuming times (from 0 min to 240 min) as a function of time during the 3rd loading stage; (d) Variation of recovery strain as a function of time during the 3rd unloading stage. The inset displays the recovery curves of MG ribbons with a resuming time of 5 min to 30 min. (In all cases the experiments were carried out at a constant temperature of 510 K and a fixed applied stress of 200 MPa after a 5 min equilibration)

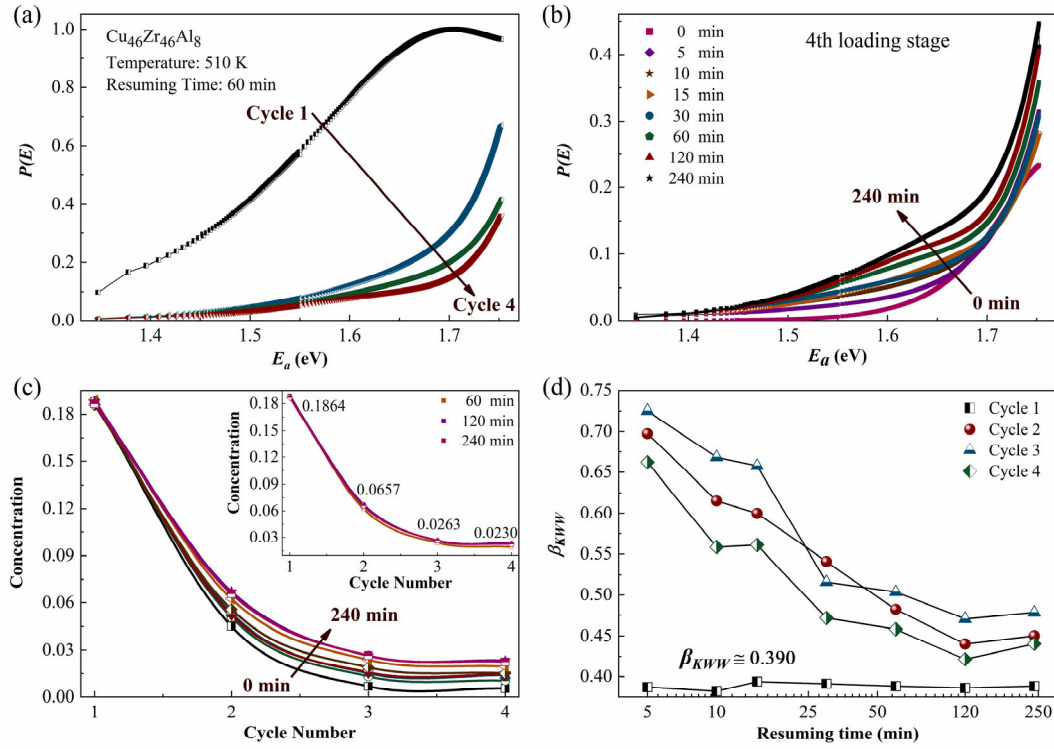


Fig. 6. (a) Normalized activation energy spectra for 4 successive cyclic loadings with a resuming time of 60 min; (b) Evolution of normalized activation energy spectra with various resuming times during the 4th loading stage; (c) Variation of relative deformation unit concentration with cycle number in the case of resuming time ranging from 0 min to 240 min. The inset highlights the variation of corresponding unit concentration with the resuming time exceeding 60 min; (d) Evolution of fitted KWW parameter β_{KWW} during creep process with various resuming times and numbers of loading cycles (from 1 to 4).

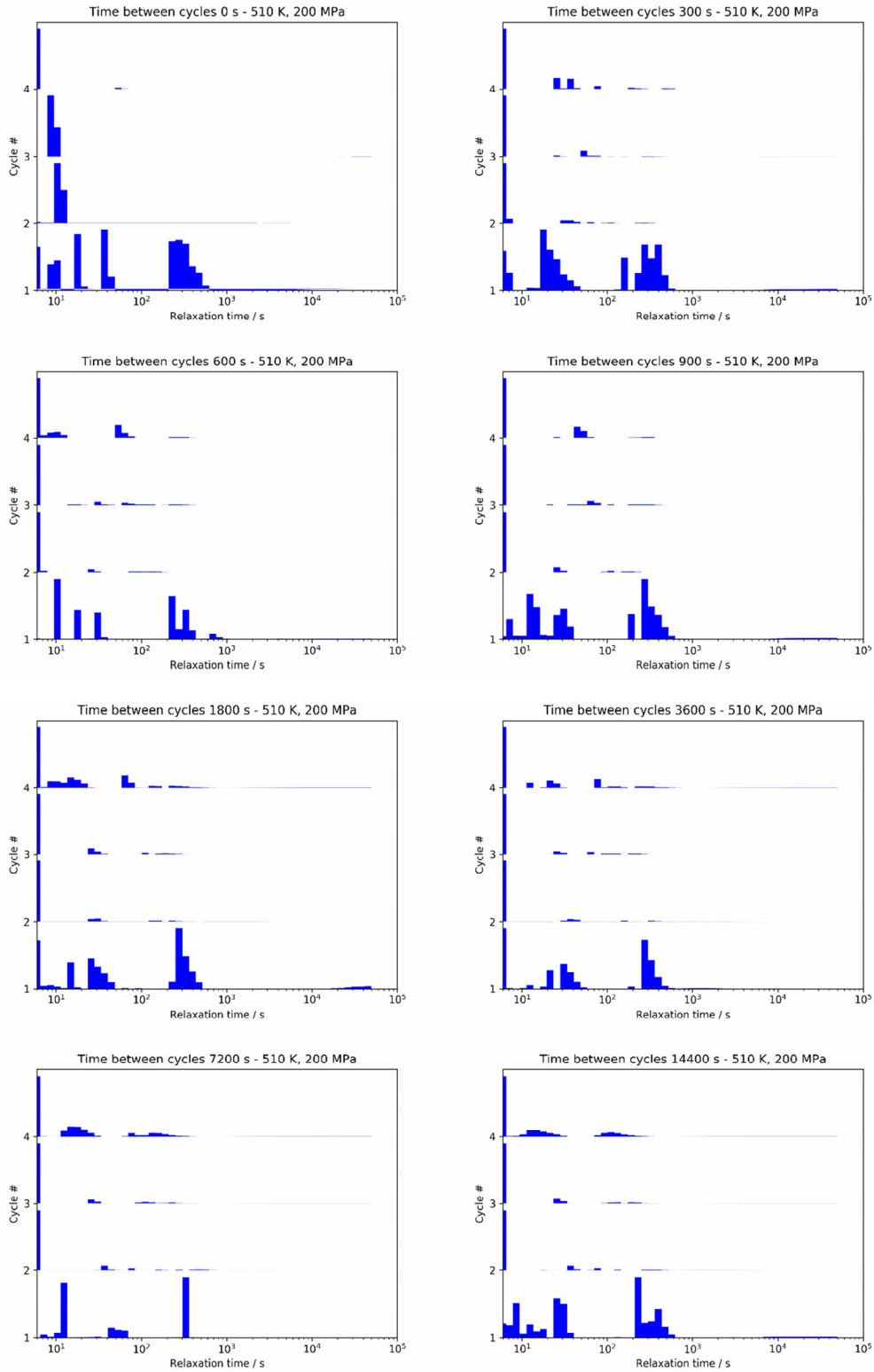


Fig. 7. Cyclic loading and resuming time adjusted relaxation time spectra of creep deformation. (All plots are scaled to the most intense peak value for clarity).

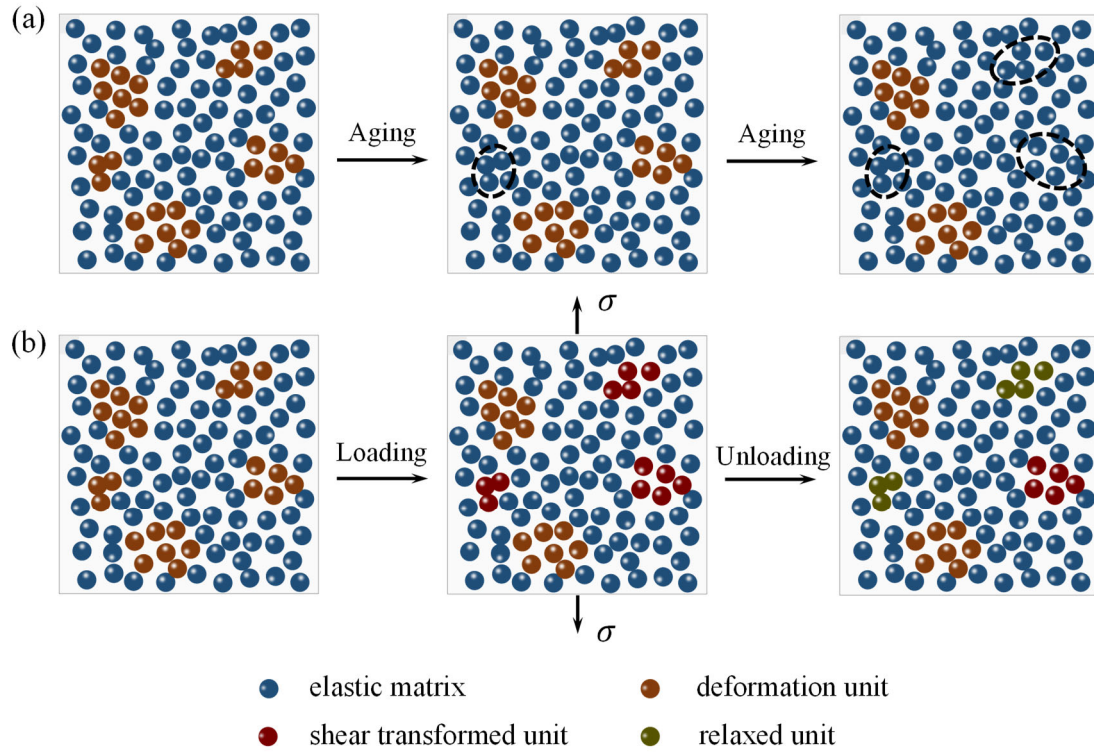


Fig. 8. Schematic illustrations of thermal and mechanical relaxations in metallic glass. (a) Annihilation of deformation units during physical aging; (b) During loading process, the deformation units become shear transformed under applied stress, a portion of which will undergo backward flipping once the stress is removed.